

Nodeless superconductivity in the noncentrosymmetric $\text{Mo}_3\text{Rh}_2\text{N}$ superconductor: a μSR study

T. Shang,^{1,2,3,*} Wensen Wei,⁴ C. Baines,⁵ J. L. Zhang,⁴ H. F. Du,⁴ M. Medarde,¹ M. Shi,² J. Mesot,^{6,3,7} and T. Shiroka^{7,6}

¹Laboratory for Multiscale Materials Experiments, Paul Scherrer Institut, Villigen CH-5232, Switzerland

²Swiss Light Source, Paul Scherrer Institut, Villigen CH-5232, Switzerland

³Institute of Condensed Matter Physics, École Polytechnique Fédérale de Lausanne (EPFL), Lausanne CH-1015, Switzerland.

⁴Anhui Province Key Laboratory of Condensed Matter Physics at Extreme Conditions,

High Magnetic Field Laboratory of the Chinese Academy of Sciences, Hefei 230026, People's Republic of China

⁵Laboratory for Muon-Spin Spectroscopy, Paul Scherrer Institut, CH-5232 Villigen PSI, Switzerland

⁶Paul Scherrer Institut, CH-5232 Villigen PSI, Switzerland

⁷Laboratorium für Festkörperphysik, ETH Zürich, CH-8093 Zurich, Switzerland

The noncentrosymmetric superconductor $\text{Mo}_3\text{Rh}_2\text{N}$, with $T_c = 4.6$ K, adopts a β -Mn-type structure (space group $P4_132$), similar to that of $\text{Mo}_3\text{Al}_2\text{C}$. Its bulk superconductivity was characterized by magnetization and heat-capacity measurements, while its microscopic electronic properties were investigated by means of muon-spin rotation and relaxation (μSR). The low-temperature superfluid density, measured via transverse-field (TF)- μSR , evidences a fully-gapped superconducting state with $\Delta_0 = 1.73 k_B T_c$, very close to $1.76 k_B T_c$ – the BCS gap value for the weak coupling case, and a magnetic penetration depth $\lambda_0 = 586$ nm. The absence of spontaneous magnetic fields below the onset of superconductivity, as determined by zero-field (ZF)- μSR measurements, hints at a preserved time-reversal symmetry in the superconducting state. Both TF- and ZF- μSR results evidence a spin-singlet pairing in $\text{Mo}_3\text{Rh}_2\text{N}$.

Introduction. The current research interest in superconductivity (SC) involves either studies of high temperature superconductors (such as cuprates or iron pnictides), or investigations of unconventional superconducting states. Superconductors with centrosymmetric crystal structures are bound to have either pure spin-singlet or spin-triplet pairings.¹ On the other hand, due to the relaxed space-symmetry requirement, noncentrosymmetric superconductors (NCSCs) may exhibit unconventional pairing.^{2,3} A lack of inversion symmetry leads to internal electric-field gradients and, hence, to antisymmetric spin-orbit coupling (ASOC), which lifts the spin degeneracy of the conduction-band electrons. As a consequence, the superconducting order can exhibit a mixture of spin-singlet and spin-triplet pairing.²⁻⁴

Of the many NCSCs known to date, however, only a few exhibit a mixed singlet-triplet pairing. $\text{Li}_2\text{Pt}_3\text{B}$ and $\text{Li}_2\text{Pd}_3\text{B}$ are two notable examples, where the mixture of singlet and triplet states can be tuned by modifying the ASOC through a Pd-for-Pt substitution.^{5,6} $\text{Li}_2\text{Pd}_3\text{B}$ behaves as a fully gapped s -wave superconductor, whereas the enhanced ASOC turns $\text{Li}_2\text{Pt}_3\text{B}$ into a nodal superconductor, with typical features of spin-triplet pairing. Other NCSCs may exhibit unconventional properties besides mixed pairing. For instance, CePt_3Si ,⁷ CeIrSi_3 ,⁸ and $\text{K}_2\text{Cr}_3\text{As}_3$,^{9,10} exhibit line nodes in the gap, while others such as LaNiC_2 ¹¹ and $(\text{La},\text{Y})_2\text{C}_3$,¹² show multiple nodeless superconducting gaps. In addition, due to the strong influence of ASOC, their upper critical fields can exceed the Pauli limit, as has been found in CePt_3Si ¹³ and $(\text{Ta},\text{Nb})\text{Rh}_2\text{B}_2$.¹⁴

$\text{Mo}_3\text{Al}_2\text{C}$ forms a β -Mn-type crystal structure with space group $P4_132$. Muon-spin rotation/relaxation (μSR), nuclear magnetic resonance (NMR), and specific heat studies have revealed that $\text{Mo}_3\text{Al}_2\text{C}$ is a fully-gapped, strongly-coupled superconductor, which preserves time-reversal symmetry (TRS) in its superconducting state.^{15,16} The recently synthesized $\text{Mo}_3\text{Rh}_2\text{N}$ NCSC, a sister compound to $\text{Mo}_3\text{Al}_2\text{C}$, has been studied via transport and specific-heat measurements.¹⁷ Yet, to date the microscopic nature of its SC state remains largely unexplored. DFT calculations suggest a strong hybridization between the Mo and Rh $4d$ -orbitals, reflecting the extended nature of the latter.¹⁸ The density of states (DOS) at the Fermi level E_F , arising from

the Rh and Mo $4d$ -orbitals, are comparable. This is in strong contrast with the $\text{Mo}_3\text{Al}_2\text{C}$ case, where the DOS at E_F is mostly dominated by Mo $4d$ -orbitals.^{15,19} In the $\text{Mo}_3\text{Rh}_2\text{N}$ case, the SOC is significantly enhanced by the replacement of a light element, such as Al, with one with a strong SOC, such as Rh. Considering that already $\text{Mo}_3\text{Al}_2\text{C}$ exhibits unusual properties,^{15,16} we expect the enhanced SOC to affect the superconducting properties of $\text{Mo}_3\text{Rh}_2\text{N}$, too. In ReT (T = transition metal) alloys,²⁰⁻²³ whose DOS is dominated by the Re $5d$ -orbitals (with negligible contributions from the T metal orbitals), even a robust increase in SOC — from $3d$ Ti to $5d$ Ta — is shown to not significantly affect the superconducting properties. Conversely, similarly to the $\text{Li}_2(\text{Pd},\text{Pt})_3\text{B}$ case, SOC effects are expected to be more important in $\text{Mo}_3\text{Rh}_2\text{N}$. Therefore, a comparative microscopic study of $\text{Mo}_3\text{Rh}_2\text{N}$ vs. $\text{Mo}_3\text{Al}_2\text{C}$ is very instructive for understanding the (A)SOC effects on the superconducting properties of NCSCs. Another goal of this study was the search for a possible TRS breaking in the superconducting state of $\text{Mo}_3\text{Rh}_2\text{N}$.

In this paper, we report on the systematic magnetization, thermodynamic, and μSR investigation of the recently discovered $\text{Mo}_3\text{Rh}_2\text{N}$ NCSC. In particular, zero- (ZF) and transverse-field (TF) μSR measurements allowed us to study the microscopic superconducting properties and to search for a possible TRS breaking below T_c in $\text{Mo}_3\text{Rh}_2\text{N}$.

Experimental details. Polycrystalline $\text{Mo}_3\text{Rh}_2\text{N}$ samples were synthesized by solid-state reaction and reductive nitridation methods, whose details are reported elsewhere.¹⁷ The room-temperature x-ray powder diffraction confirmed the β -Mn-type crystal structure, with no detectable extra phases.¹⁷ The magnetization and heat capacity measurements were performed on a 7-T Quantum Design Magnetic Property Measurement System (MPMS) and a 9-T Physical Property Measurement System (PPMS). The bulk μSR measurements were carried out using the general-purpose surface-muon (GPS) and the low-temperature facility (LTF) instruments of the $\pi\text{M}3$ beamline at the Swiss muon source of Paul Scherrer Institut, Villigen, Switzerland. For measurements on LTF, the samples were mounted on a silver plate using diluted GE varnish. The μSR data were analyzed by means of the `musrfit` software package.²⁴

Characterizing bulk superconductivity. The magnetic sus-

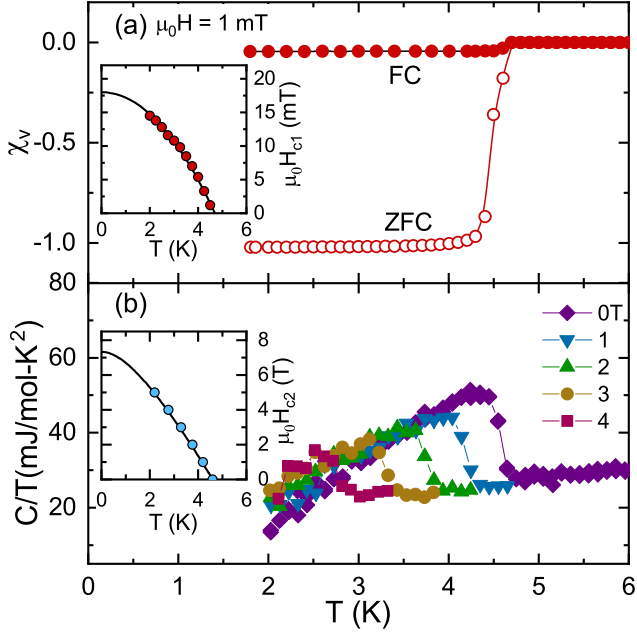


FIG. 1. (a) Temperature dependence of magnetic susceptibility $\chi(T)$ and (b) of specific heat $C(T)/T$ for $\text{Mo}_3\text{Rh}_2\text{N}$. The inset in (a) shows the estimated $\mu_0 H_{c1}$ vs. temperature up to T_c , the solid-line being a fit to $\mu_0 H_{c1}(T) = \mu_0 H_{c1}(0)[1 - (T/T_c)^2]$. For each temperature, $\mu_0 H_{c1}$ was determined from the value where $M(H)$ deviates from linearity. The inset in (b) shows $\mu_0 H_{c2}(T)$, as determined from heat-capacity measurements in various applied fields, with the solid-line being a fit to the WHH model without spin-orbit scattering.

ceptibility of $\text{Mo}_3\text{Rh}_2\text{N}$ was measured using both field-cooled (FC) and zero-field-cooled (ZFC) protocols in an applied field of 1 mT. As shown in Fig. 1(a), the ZFC-susceptibility indicates bulk superconductivity below $T_c = 4.6$ K in $\text{Mo}_3\text{Rh}_2\text{N}$, consistent with the previously reported value.¹⁷ The lower critical field $\mu_0 H_{c1}$ was determined from the field-dependent magnetization $M(H)$, measured at various temperatures below T_c . The estimated $\mu_0 H_{c1}(T)$ values are shown in the inset of Fig. 1(a). The solid-line represents a fit to $\mu_0 H_{c1}(T) = \mu_0 H_{c1}(0)[1 - (T/T_c)^2]$ and yields a lower critical field $\mu_0 H_{c1}(0) = 18(1)$ mT. The bulk superconductivity of $\text{Mo}_3\text{Rh}_2\text{N}$ was further confirmed by heat capacity measurements [see Fig. 1(b)]. The specific heat, too, exhibits a sharp transition at T_c , which shifts towards lower temperature upon increasing the magnetic field. The sharp transitions ($\Delta T \sim 0.3$ K) in both the specific-heat and magnetic-susceptibility data indicate a good sample quality. The derived T_c values vs. the applied field are summarized in the inset of Fig. 1(b), from which the upper critical field $\mu_0 H_{c2}$ was determined following the Werthamer-Helfand-Hohenberg (WHH) model.²⁵ The solid-line in the inset of Fig. 1(b) represents a fit to the WHH model, without considering spin-orbital scattering, and gives $\mu_0 H_{c2}(0) = 7.32(1)$ T, consistent with the previously reported value.¹⁷

Transverse-field μSR . To explore the microscopic superconducting properties of $\text{Mo}_3\text{Rh}_2\text{N}$, TF- μSR measurements were performed down to 0.02 K. In order to track the additional field-distribution broadening due to the flux-line-lattice (FLL) in the mixed superconducting state, a magnetic field of 30 mT [i.e., larger than the lower critical field $\mu_0 H_{c1}(0)$] was applied at temperatures above T_c . The TF- μSR time spectra were collected at various temperatures up

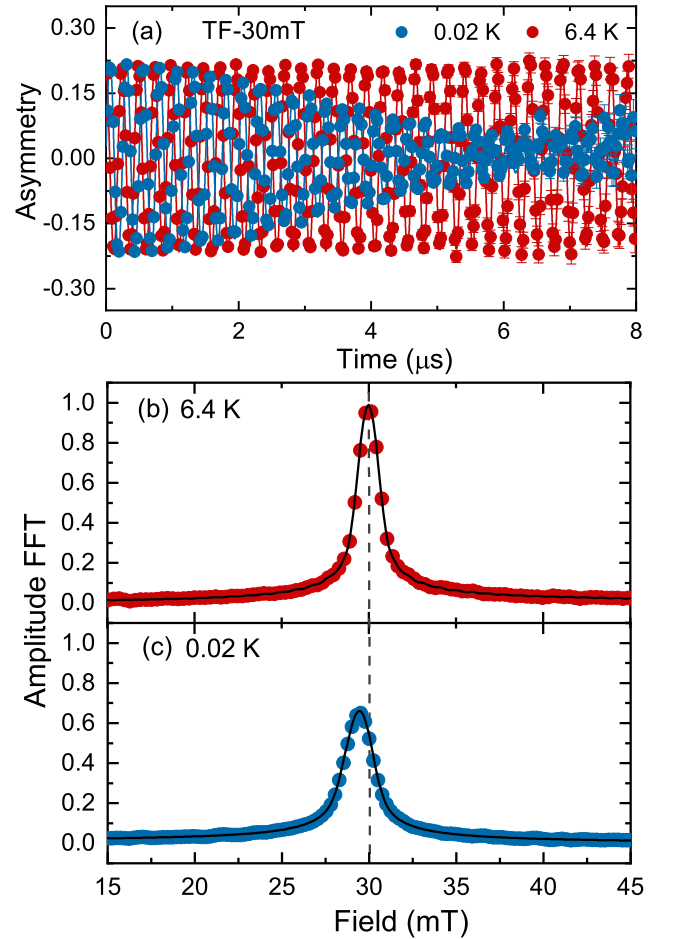


FIG. 2. (a) The $\text{Mo}_3\text{Rh}_2\text{N}$ TF- μSR time spectra, collected at 0.02 K and 6.4 K in an applied field of 30 mT, show very different relaxation rates. Fourier transforms of the above time spectra at 6.4 K (b) and 0.02 K (c). The solid lines are fits to Eq. (1) using a single Gaussian relaxation; the dashed lines indicate the applied magnetic field. Note the clear diamagnetic shift below T_c in (c).

to T_c , following a field-cooling protocol. Figure 2(a) shows two representative TF- μSR spectra collected above (6.4 K) and below T_c (0.02 K) on GPS and LTF, respectively. The observed phase shift between the two datasets is due to instrumental effects. The faster, FLL-induced decay in the superconducting state is clearly seen in the second case. The time evolution of the μSR -asymmetry is modeled by:

$$A_{\text{TF}} = A_s \cos(\gamma_\mu B_s t + \phi) e^{-\sigma^2 t^2 / 2} + A_{\text{bg}} \cos(\gamma_\mu B_{\text{bg}} t + \phi). \quad (1)$$

Here A_s and A_{bg} represent the initial muon-spin asymmetries for muons implanted in the sample and sample holder, respectively, with the latter not undergoing any depolarization. The A_s/A_{TF} ratios were determined from the long-time tail of TF- μSR spectra at base temperature [see Fig. 2(a)],²⁶ and fixed to 0.88 (GPS) and 0.90 (LTF) for all the temperatures. B_s and B_{bg} are the local fields sensed by implanted muons in the sample and sample holder, $\gamma_\mu = 2\pi \times 135.53$ MHz/T is the muon gyromagnetic ratio, ϕ is the shared initial phase, and σ is a Gaussian relaxation rate. The Gaussian nature of relaxation is clearly evinced from the fast-Fourier-transform (FFT) spectra shown in Fig. 2(b) and (c). In the mixed superconducting state, the faster decay of muon-spin polarization reflects the inhomogeneous field distribution due to the FLL, which causes

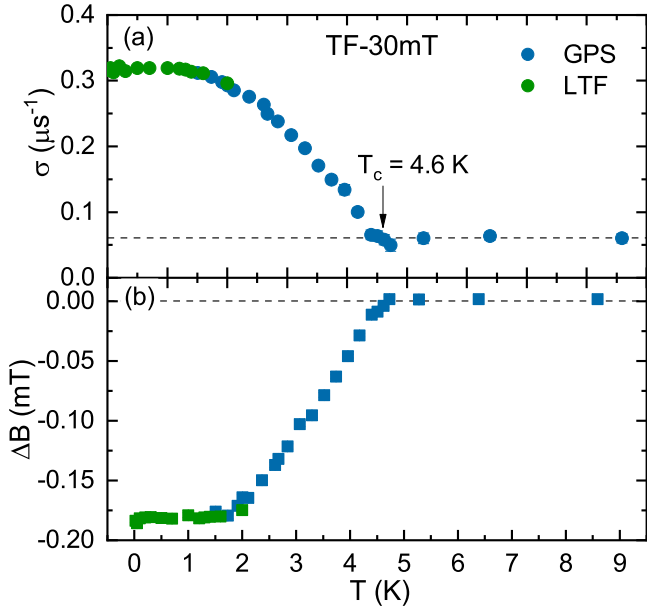


FIG. 3. Temperature dependence of (a) the muon-spin relaxation rate $\sigma(T)$ and (b) diamagnetic field shift $\Delta B(T)$ for $\text{Mo}_3\text{Rh}_2\text{N}$ measured in an applied field of 30 mT. Here $\Delta B = B_s - B_{\text{bg}}$, where B_{bg} is the same as the applied magnetic field.

the additional distribution broadening in the mixed state [see Fig. 2(c)]. In the superconducting state, the measured Gaussian relaxation rate includes contributions from both a temperature-independent relaxation due to nuclear moments (σ_n) and the FLL (σ_{sc}). The FLL-related relaxation can be extracted by subtracting the nuclear contribution according to $\sigma_{\text{sc}} = \sqrt{\sigma^2 - \sigma_n^2}$. The derived Gaussian relaxation rate and the diamagnetic field shift as a function of temperature are summarized in Fig. 3. The relaxation rate, shown in Fig. 3(a), is small and independent of temperature for $T > T_c$, but it starts to increase below T_c , indicating the onset of FLL and an increase in superfluid density. Concomitantly, a diamagnetic field shift appears below T_c [see Fig. 3(b)].

Since σ_{sc} is directly related to the magnetic penetration depth and the superfluid density ($\sigma_{\text{sc}} \propto 1/\lambda^2$), the superconducting gap value and its symmetry can be determined from the measured $\sigma_{\text{sc}}(T)$. For small applied magnetic fields [$H_{\text{appl}}/H_{c2} \sim 0.004 \ll 1$], the magnetic penetration depth λ can be calculated from:^{27,28}

$$\frac{\sigma_{\text{sc}}^2(T)}{\gamma_{\mu}^2} = 0.00371 \frac{\Phi_0^2}{\lambda^4(T)}. \quad (2)$$

Figure 4 shows the inverse square of the magnetic penetration depth (proportional to the superfluid density) as a function of temperature for $\text{Mo}_3\text{Rh}_2\text{N}$. To gain insight into the SC pairing symmetry in $\text{Mo}_3\text{Rh}_2\text{N}$, its temperature-dependent superfluid density $\rho_{\text{sc}}(T)$ was further analyzed by using different models, generally described by:

$$\rho_{\text{sc}}(T) = 1 + 2 \left\langle \int_{\Delta_{\mathbf{k}}}^{\infty} \frac{E}{\sqrt{E^2 - \Delta_{\mathbf{k}}^2}} \frac{\partial f}{\partial E} dE \right\rangle_{\text{FS}}, \quad (3)$$

where $\Delta_{\mathbf{k}}$ is an angle-dependent gap function, $f = (1 + e^{E/k_B T})^{-1}$ is the Fermi function, and $\langle \rangle_{\text{FS}}$ represents an average over the Fermi surface.²⁹ The gap function can be

written as $\Delta_{\mathbf{k}}(T) = \Delta(T)g_{\mathbf{k}}$, where Δ is the maximum gap value and $g_{\mathbf{k}}$ is the angular dependence of the gap, equal to 1, $\cos 2\psi$, and $\sin \theta$ for an s -, d -, and p -wave model, respectively. Here ψ and θ are azimuthal angles. The

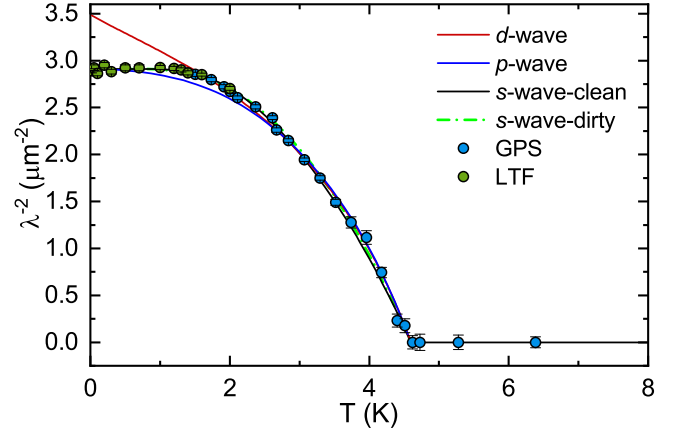


FIG. 4. Superfluid density vs. temperature, as determined from TF- μ SR measurements. The different lines represent fits to various models, including s -, d -, and p -wave pairing (see text for details).

temperature dependence of the gap is assumed to follow $\Delta(T) = \Delta_0 \tanh\{1.82[1.018(T_c/T - 1)]^{0.51}\}$,²⁹ where Δ_0 , the gap value at zero temperature, is the only adjustable parameter. Note that the function $\Delta(T)$ is practically independent of the different models.

Three different models, including s -, d -, and p waves, were used to describe the temperature-dependent superfluid density $\lambda^{-2}(T)$. By fixing the zero-temperature magnetic penetration depth $\lambda_0 = 586(3)$ nm, the estimated gap values for the s - and p -wave model are 0.76(1) and 1.07(1) meV, respectively; while for the d -wave model, the estimated λ_0 and gap value are 536(3) nm and 1.11(1) meV. As can be seen in Fig. 4, the temperature dependence of the superfluid density is clearly consistent with a single fully-gapped s -wave model. In case of d - or p -wave models, a poor agreement with the measured λ^{-2} values is found, especially at low temperature. The s -wave nature of SC is further confirmed by the temperature-independent behavior of $\lambda^{-2}(T)$ for $T < 1/3T_c$, which strongly suggests a nodeless superconductivity in $\text{Mo}_3\text{Rh}_2\text{N}$. Such conclusion is supported also by low- T specific-heat data.¹⁷

Unlike the clean-limit case [see Eq. (3)], in the dirty limit the coherence length ξ is much larger than the electronic mean-free path l_e . In this case, in the BCS approximation, the temperature dependence of the superfluid density is given by:²⁹

$$\rho_{\text{sc}}(T) = \frac{\Delta(T)}{\Delta_0} \tanh \left[\frac{\Delta(T)}{2k_B T} \right]. \quad (4)$$

Following the above equation, the estimated gap value is 0.68(1) meV, slightly smaller than the clean-limit value, yet still in excellent agreement with the gap values extracted from low- T specific-heat (0.67 meV) and Andreev-reflection spectroscopy data (0.59 meV).¹⁷ Such ‘dirty’ nature of SC might reflect the large electrical resistivity ($\rho_0 = 0.48$ m Ω cm) and the small residual resistivity ratio (RRR ~ 1) of $\text{Mo}_3\text{Rh}_2\text{N}$. The $2\Delta/k_B T_c$ ratios of about 3.46 (dirty limit) and 3.84 (clean limit) are both comparable to 3.53, the ideal value expected for a weakly-coupled BCS superconductor.

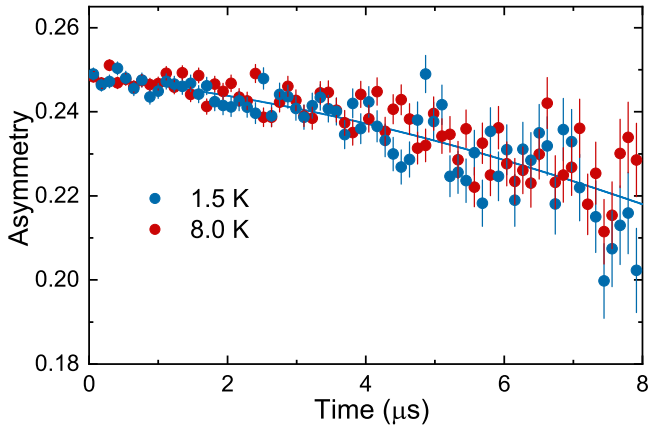


FIG. 5. Coinciding ZF- μ SR spectra in the superconducting (1.5 K) and the normal state (8 K) show that in $\text{Mo}_3\text{Rh}_2\text{N}$ the TRS is preserved. Both spectra show only a weak muon-spin depolarization, but no visible differences. The solid line is a fit to the 1.5-K spectra by means of Eq. (5), as described in the text.

Zero-field μ SR. We performed also ZF- μ SR measurements, in order to search for a possible TRS breaking in the superconducting state of $\text{Mo}_3\text{Rh}_2\text{N}$. The large muon gyromagnetic ratio, combined with the availability of 100% spin-polarized muon beams, make ZF- μ SR a very sensitive probe for detecting small spontaneous magnetic fields. This technique has been successfully used to detect the TRS breaking in the superconducting states of different types of materials.^{20,22,30–33} Normally, in the absence of external fields, the onset of SC does not imply changes in the ZF muon-spin relaxation rate. However, if the TRS is broken, the onset of tiny spontaneous currents gives rise to associated (weak) magnetic fields, readily detected by ZF- μ SR as an increase in muon-spin relaxation rate. Given the tiny size of such effects, we measured the ZF- μ SR with high statistics in both the normal and the superconducting phases. Representative ZF- μ SR spectra collected above (8 K) and below (1.5 K) T_c for $\text{Mo}_3\text{Rh}_2\text{N}$ are shown in Fig. 5. For non-magnetic materials, in the absence of applied fields, the relaxation is mainly determined by the randomly oriented nuclear moments, which can be described by a Gaussian Kubo-Toyabe relaxation function $G_{\text{KT}} = \left[\frac{1}{3} + \frac{2}{3}(1 - \sigma^2 t^2) e^{-\frac{\sigma^2 t^2}{2}} \right]$.^{34,35} The ZF- μ SR spectra of $\text{Mo}_3\text{Rh}_2\text{N}$ can be modeled by adding a Lorentzian relaxation Λ to the Kubo-Toyabe function:

$$A_{\text{ZF}} = A_s G_{\text{KT}} e^{-\Lambda t} + A_{\text{bg}}. \quad (5)$$

Here A_s and A_{bg} are the same as in the TF- μ SR case [see Eq. (1)]. The resulting fit parameters are summarized in Table I. The weak Gaussian and Lorentzian relaxation rates reflect the small value of $\text{Mo}_3\text{Rh}_2\text{N}$ nuclear moments. The relaxations show very similar values in both the normal and the superconducting phase, as demonstrated by a lack of vis-

ible differences in the ZF- μ SR spectra above and below T_c . This lack of evidence for an additional μ SR relaxation below T_c , implies that TRS is preserved in the superconducting state of $\text{Mo}_3\text{Rh}_2\text{N}$. Since TRS is preserved also in the $\text{Mo}_3\text{Al}_2\text{C}$ sister compound, this explains the many common features shared by these two β -Mn-type NCSCs.¹⁶

Discussion. Since the admixture of spin-singlet and spin-triplet pairing depends on the strength of ASOC,⁴ the latter plays an important role in determining the superconduct-

Table I. Fit parameters extracted from ZF- μ SR data for $\text{Mo}_3\text{Rh}_2\text{N}$ (collected above and below T_c) by using the Eq. (5) model.

Temperature	1.5 K	8 K
A_s	0.24814(83)	0.24833(73)
σ (μs^{-1})	0.0366(69)	0.0379(58)
Λ (μs^{-1})	0.0069(32)	0.0047(28)
A_{bg}	0.01985(83)	0.01987(73)

ing properties of NCSCs. An enhanced ASOC can turn a fully gapped s -wave superconductor into a nodal superconductor, with typical features of spin-triplet pairing, as exemplified by the $\text{Li}_2(\text{Pd,Pt})_3\text{B}$ case. However, a larger SOC is not necessarily the only requirement for a larger ASOC and an enhanced band splitting E_{ASOC} , since the latter two depend also on the specific crystal- and electronic structures. All 4d-Rh, -Ru and 5d-Ir are heavy SOC metals, but their ASOC-related band splittings E_{ASOC} are relatively small in some materials. For example, the expected E_{ASOC} values for $\text{Ce}(\text{Rh,Ir})\text{Si}_3$, LaRhSi_3 , Rh_2Ga_9 , and Ru_7B_3 are less than 20 meV (i.e., ten times smaller than in CePt_3Si or $\text{Li}_2\text{Pt}_3\text{B}$).³ Therefore, their pairing states remain in the spin-singlet channel and all of them behave as fully-gapped superconductors. In β -Mn-type materials, like $\text{Mo}_3\text{Rh}_2\text{N}$, the replacement of a light metal such as Al by the heavy Rh does indeed increase the SOC, yet the E_{ASOC} still remains weak. Hence, the superconducting pairing is of spin-singlet type, in good agreement with both TF- and ZF- μ SR results. Further band structure calculations, which explicitly take into account the SOC effects, are needed to clarify this behavior.

Summary. We performed comparative μ SR experiments to study the superconducting properties of NCSC $\text{Mo}_3\text{Rh}_2\text{N}$. Bulk superconductivity with $T_c = 4.6$ K was characterized by magnetization and heat capacity measurements. The temperature variation of the superfluid density reveals nodeless superconductivity in $\text{Mo}_3\text{Rh}_2\text{N}$, which is well described by an isotropic s -wave model and is consistent with a spin-singlet pairing. The lack of spontaneous magnetic fields below T_c indicates that time-reversal symmetry is preserved in the superconducting state of $\text{Mo}_3\text{Rh}_2\text{N}$.

This work was supported by the Schweizerische Nationalfonds zur Förderung der Wissenschaftlichen Forschung, SNF (Grants 200021-169455 and 206021-139082) and the National Natural Science Foundation of China (Grant No. 11504378).

* Corresponding authors:
tian.shang@psi.ch

¹ P. W. Anderson, “Structure of “triplet” superconducting energy gaps,” *Phys. Rev. B* **30**, 4000–4002 (1984).

² E. Bauer and M. Sigrist, eds., *Non-Centrosymmetric Supercon-*

ductors, Vol. 847 (Springer Verlag, Berlin, 2012).

³ M. Smidman, M. B. Salamon, H. Q. Yuan, and D. F. Agterberg, “Superconductivity and spin-orbit coupling in non-centrosymmetric materials: A review,” *Rep. Prog. Phys.* **80**, 036501 (2017), and references therein.

- ⁴ L. P. Gor'kov and E. I. Rashba, "Superconducting 2D system with lifted spin degeneracy: Mixed singlet-triplet state," *Phys. Rev. Lett.* **87**, 037004 (2001).
- ⁵ H. Q. Yuan, D. F. Agterberg, N. Hayashi, P. Badica, D. Vandervelde, K. Togano, M. Sigris, and M. B. Salamon, "*s*-wave spin-triplet order in superconductors without inversion symmetry: $\text{Li}_2\text{Pd}_3\text{B}$ and $\text{Li}_2\text{Pt}_3\text{B}$," *Phys. Rev. Lett.* **97**, 017006 (2006).
- ⁶ M. Nishiyama, Y. Inada, and Guo-qing Zheng, "Spin triplet superconducting state due to broken inversion symmetry in $\text{Li}_2\text{Pt}_3\text{B}$," *Phys. Rev. Lett.* **98**, 047002 (2007).
- ⁷ I. Bonalde, W. Brämer-Escamilla, and E. Bauer, "Evidence for line nodes in the superconducting energy gap of noncentrosymmetric CePt_3Si from magnetic penetration depth measurements," *Phys. Rev. Lett.* **94**, 207002 (2005).
- ⁸ H. Mukuda, T. Fujii, T. Ohara, A. Harada, M. Yashima, Y. Kitaoka, Y. Okuda, R. Settai, and Y. Onuki, "Enhancement of superconducting transition temperature due to the strong antiferromagnetic spin fluctuations in the noncentrosymmetric heavy-fermion superconductor CeIrSi_3 : A ^{29}Si NMR study under pressure," *Phys. Rev. Lett.* **100**, 107003 (2008).
- ⁹ G. M. Pang, M. Smidman, W. B. Jiang, J. K. Bao, Z. F. Weng, Y. F. Wang, L. Jiao, J. L. Zhang, G. H. Cao, and H. Q. Yuan, "Evidence for nodal superconductivity in quasi-one-dimensional $\text{K}_2\text{Cr}_3\text{As}_3$," *Phys. Rev. B* **91**, 220502 (2015).
- ¹⁰ D. T. Adroja, A. Bhattacharyya, M. Telling, Yu. Feng, M. Smidman, B. Pan, J. Zhao, A. D. Hillier, F. L. Pratt, and A. M. Strydom, "Superconducting ground state of quasi-one-dimensional $\text{K}_2\text{Cr}_3\text{As}_3$ investigated using μSR measurements," *Phys. Rev. B* **92**, 134505 (2015).
- ¹¹ J. Chen, L. Jiao, J. L. Zhang, Y. Chen, L. Yang, M. Nicklas, F. Steglich, and H. Q. Yuan, "Evidence for two-gap superconductivity in the non-centrosymmetric compound LaNiC_2 ," *New J. Phys.* **15**, 053005 (2013).
- ¹² S. Kuroiwa, Y. Saura, J. Akimitsu, M. Hiraishi, M. Miyazaki, K. H. Satoh, S. Takeshita, and R. Kadono, "Multigap superconductivity in sesquicarbides La_2C_3 and Y_2C_3 ," *Phys. Rev. Lett.* **100**, 097002 (2008).
- ¹³ E. Bauer, G. Hilscher, H. Michor, C. Paul, E. W. Scheidt, A. Gribanov, Y. Seropugin, H. Noël, M. Sigris, and P. Rogl, "Heavy fermion superconductivity and magnetic order in noncentrosymmetric CePt_3Si ," *Phys. Rev. Lett.* **92**, 027003 (2004).
- ¹⁴ E. M. Carnicom, W. W. Xie, T. Klimczuk, J. J. Lin, K. Górnicka, Z. Sobczak, N. P. Ong, and R. J. Cava, " TaRh_2B_2 and NbRh_2B_2 : Superconductors with a chiral noncentrosymmetric crystal structure," *Sci. Adv.* **4**, 7969 (2018).
- ¹⁵ E. Bauer, G. Rogl, Xing-Qiu Chen, R. T. Khan, H. Michor, G. Hilscher, E. Royanian, K. Kumagai, D. Z. Li, Y. Y. Li, R. Podloucky, and P. Rogl, "Unconventional superconducting phase in the weakly correlated noncentrosymmetric $\text{Mo}_3\text{Al}_2\text{C}$ compound," *Phys. Rev. B* **82**, 064511 (2010).
- ¹⁶ E. Bauer, C. Sekine, U. Sai, P. Rogl, P. K. Biswas, and A. Amato, "Absence of time-reversal symmetry breaking in the noncentrosymmetric superconductor $\text{Mo}_3\text{Al}_2\text{C}$," *Phys. Rev. B* **90**, 054522 (2014).
- ¹⁷ Wensen Wei, G. J. Zhao, D. R. Kim, Chiming Jin, J. L. Zhang, Langsheng Ling, Lei Zhang, Haifeng Du, T. Y. Chen, Jiadong Zang, Mingliang Tian, C. L. Chien, and Yuheng Zhang, " $\text{Rh}_2\text{Mo}_3\text{N}$: Noncentrosymmetric *s*-wave superconductor," *Phys. Rev. B* **94**, 104503 (2016).
- ¹⁸ Wei Li, Chiming Jin, Renchao Che, Wensen Wei, Langsheng Lin, Lei Zhang, Haifeng Du, Mingliang Tian, and Jiadong Zang, "Emergence of skyrmions from rich parent phases in the molybdenum nitrides," *Phys. Rev. B* **93**, 060409 (2016).
- ¹⁹ A. B. Karki, Y. M. Xiong, I. Vekhter, D. Browne, P. W. Adams, D. P. Young, K. R. Thomas, Julia Y. Chan, H. Kim, and R. Prozorov, "Structure and physical properties of the noncentrosymmetric superconductor $\text{Mo}_3\text{Al}_2\text{C}$," *Phys. Rev. B* **82**, 064512 (2010).
- ²⁰ R. P. Singh, A. D. Hillier, B. Mazidian, J. Quintanilla, J. F. Annett, D. McK. Paul, G. Balakrishnan, and M. R. Lees, "Detection of time-reversal symmetry breaking in the noncentrosymmetric superconductor Re_6Zr using muon-spin spectroscopy," *Phys. Rev. Lett.* **112**, 107002 (2014).
- ²¹ D. Singh, J. A. T. Barker, A. Thamizhavel, D. McK. Paul, A. D. Hillier, and R. P. Singh, "Time-reversal symmetry breaking in the noncentrosymmetric superconductor Re_6Hf : Further evidence for unconventional behavior in the α -Mn family of materials," *Phys. Rev. B* **96**, 180501 (2017).
- ²² T. Shang, G. M. Pang, C. Baines, W. B. Jiang, W. Xie, A. Wang, M. Medarde, E. Pomjakushina, M. Shi, J. Mesot, H. Q. Yuan, and T. Shiroka, "Nodeless superconductivity and time-reversal symmetry breaking in the noncentrosymmetric superconductor Re_{24}Ti ," *Phys. Rev. B* **97**, 020502 (2018).
- ²³ J. A. T. Barker, B. D. Breen, R. Hanson, A. D. Hillier, M. R. Lees, G. Balakrishnan, D. McK. Paul, and R. P. Singh, "Superconducting and normal-state properties of the noncentrosymmetric superconductor Re_3Ta ," *Phys. Rev. B* **98**, 104506 (2018).
- ²⁴ A. A. Suter and B. M. Wojek, "Musrfit: A free platform-independent framework for μSR data analysis," *Phys. Procedia* **30**, 69 (2012).
- ²⁵ N. R. Werthamer, E. Helfand, and P. C. Hohenberg, "Temperature and purity dependence of the superconducting critical field, H_{c2} . III. Electron spin and spin-orbit effects," *Phys. Rev.* **147**, 295 (1966).
- ²⁶ Due to the complete decay of the sample-related asymmetry beyond $7\mu\text{s}$, the residual signal is due to the background only.
- ²⁷ W. Barford and J. M. F. Gunn, "The theory of the measurement of the London penetration depth in uniaxial type II superconductors by muon spin rotation," *Physica C* **156**, 515 (1988).
- ²⁸ E. H. Brandt, "Properties of the ideal Ginzburg-Landau vortex lattice," *Phys. Rev. B* **68**, 054506 (2003).
- ²⁹ M. Tinkham, *Introduction to superconductivity* (Courier Corporation, 1996).
- ³⁰ A. D. Hillier, J. Quintanilla, and R. Cywinski, "Evidence for time-reversal symmetry breaking in the noncentrosymmetric superconductor LaNiC_2 ," *Phys. Rev. Lett.* **102**, 117007 (2009).
- ³¹ J. A. T. Barker, D. Singh, A. Thamizhavel, A. D. Hillier, M. R. Lees, G. Balakrishnan, D. McK. Paul, and R. P. Singh, "Unconventional superconductivity in La_7Ir_3 revealed by muon spin relaxation: Introducing a new family of noncentrosymmetric superconductor that breaks time-reversal symmetry," *Phys. Rev. Lett.* **115**, 267001 (2015).
- ³² G. M. Luke, Y. Fudamoto, K. M. Kojima, M. I. Larkin, J. Merrin, B. Nachumi, Y. J. Uemura, Y. Maeno, Z. Q. Mao, Y. Mori, H. Nakamura, and M. Sigris, "Time-reversal symmetry-breaking superconductivity in Sr_2RuO_4 ," *Nature* **394**, 558 (1998).
- ³³ Y. Aoki, A. Tsuchiya, T. Kanayama, S. R. Saha, H. Sugawara, H. Sato, W. Higemoto, A. Koda, K. Ohishi, K. Nishiyama, and R. Kadono, "Time-reversal symmetry-breaking superconductivity in heavy-fermion $\text{PrOs}_4\text{Sb}_{12}$ detected by muon-spin relaxation," *Phys. Rev. Lett.* **91**, 067003 (2003).
- ³⁴ R. Kubo and T. Toyabe, *Magnetic Resonance and Relaxation*, edited by R. Blinc (North-Holland, Amsterdam, 1967).
- ³⁵ A. Yaouanc and P. Dalmas de Réotier, *Muon Spin Rotation, Relaxation, and Resonance: Applications to Condensed Matter* (Oxford University Press, Oxford, 2011).